Journal of Alloys and Compounds 509 (2011) 6652–6658

Contents lists available at ScienceDirect

Journal of Alloys and Compounds

journal homepage: www.elsevier.com/locate/jallcom

# Structure and electrical properties of $MnO_2$-doped $Sr_{2-x}Ca_xNaNb_5O_{15}$ lead-free piezoelectric ceramics

Xiujun Fan [a,*], Yue Wang [a], Yijian Jiang [b]

[a] College of Applied Sciences, Beijing University of Technology, Beijing 100124, China
[b] Institute of Laser Engineering, Beijing University of Technology, Beijing 100124, China

ARTICLE INFO

*Article history:*
Received 23 November 2010
Received in revised form 27 January 2011
Accepted 20 March 2011
Available online 30 March 2011

*Keywords:*
Piezoelectric ceramics
Dielectric properties
Tungsten–bronze
Relaxor ferroelectric

ABSTRACT

Lead-free piezoelectric ceramics $Sr_{2-x}Ca_xNaNb_5O_{15} + y$ wt% $MnO_2$ have been prepared by the conventional solid state reaction method. Our results reveal that $Ca^{2+}$ and Mn ions have entered into the $Sr_2NaNb_5O_{15}$ lattices to form a solid solution with tungsten–bronze structure. The substitution of $Ca^{2+}$ induces a decrease in piezoelectric coefficient $d_{33}$, electromechanical coupling factors $k_p$ and $k_t$, while, the addition of Mn ions decreases the sintering temperature and effectively promotes the densification of the ceramics. The effect of substitution of $Ca^{2+}$ and Mn ions on the structure, electrical properties and diffused phase changing were investigated systematically. For the ceramic with $x = 0.05$ and $y = 0.5$, the piezoelectric, dielectric and ferroelectric properties become optimum, giving a piezoelectric coefficient $d_{33} = 190$ pC/N, electromechanical coupling factors $k_p = 13.4\%$ and $k_t = 36.5\%$, $\varepsilon_r = 2123$, loss tangent $\tan\delta = 0.038$, remanent polarization $P_r = 4.76\ \mu C/cm^2$, coercive field $E_c = 12.68$ kV/cm, and Curie temperature $T_c = 260\ ^\circ C$.



## 1. Introduction

Lead–zirconium–titanium (PZT) based piezoceramics have excellent piezoelectric properties and hence have been widely used in the manufacture of actuators, sensors, transducers and other electromechanical devices. However, the use of the lead-based ceramics has caused serious environmental problem because of the toxicity of lead oxide and its high vapor pressure during processing [1]. Therefore, it is urgent to develop environmental benign alternative materials [2]. In recent years, a number of extensive studies on lead-free piezoelectric ceramics such as $Bi_{0.5}Na_{0.5}TiO_3$-based ceramics [3,4], Bi-layered structure materials [5], tungsten–bronze-type materials [6,7], $BaTiO_3$-based ceramics [8], and alkaline niobate-based materials [9,10] have been carried out. One of the lead-free ferroelectric oxides, mixed niobates with tungsten–bronze (TB) structure have received considerable attention owing to their potential applications as ferroelectric, piezoelectric, nonlinear optic and pyroelectric materials because of their large spontaneous polarization, high piezoelectric, electric–optic and pyroelectric coefficient [11,12]. Among these tungsten–bronze niobates, $Sr_{2-x}Ca_xNaNb_5O_{15}$ (abbreviated as SCNN), with high Curie temperature $T_c$ (about 300 °C), large crystalline anisotropy and high piezoelectric properties along the *c*-axis of the crystal structure have received increasing interests. The single crystals of SCNN have already been synthesized by Neurgaonkar et al., and found they have relatively large and nearly equal longitudinal ($d_{33} = 270$ pC/N) and shear ($d_{15} = 248$ pC/N) piezoelectric coefficients [13]. However, it is difficult to obtain sufficiently large single crystal of SCNN. At the same time, polycrystalline ceramics having many advantages over single crystals, such as low cost, ease of fabrication, large size, and isotropic properties. However, there are still many difficulties encountered during producing tungsten–bronze ferroelectric ceramics (e.g., $Ba_xSr_{5-x}Nb_{10}O_{30}$ [14], $KSr_2NaNB_5O_{15}$ [15], and $(Pb_{1-x}Ba_x)Nb_2O_6$ [16], such as abnormal grain growth, crack generation and pore formation. In order to produce pore-free and high-density SCNN ceramics, several strategies have been used, including spark plasma sintering (SPS) [17,18].

$MnO_2$ is one of the most interesting and useful additives, because Mn ions have multivalence: $Mn^{2+}$, $Mn^{3+}$, and $Mn^{4+}$. When Mn ions are used to substitute the metal cations in perovskite-type $ABO_3$ ferroelectric materials, they generally substitute cations with similar ionic radii in the A or B site [9]. In the lead–zirconium–titanium (PZT) [19,20] and barium–titanium (BT) [21] based piezoelectric ceramics, $MnO_2$ additive is usually recognized as an acceptor or "hard" doping element. On the other hand, Mn doping can cause "soft" and "hard" effects simultaneously in PZT ceramics, when the Mn doping ratio is at an optimum content [22]. However, the effects of Mn doping in the tungsten–bronze structure compounds have not been studied extensively as much as that in PZT-based or BT-based ferroelectric ceramics. In the present work,

* Corresponding author. Tel.: +86 10 67392201; fax: +86 10 67392030.
*E-mail address:* fxiujun@gmail.com (X. Fan).

0925-8388/$ – see front matter © 2011 Elsevier B.V. All rights reserved.
doi:10.1016/j.jallcom.2011.03.130

$MnO_2$ doped $Sr_{2-x}Ca_xNaNb_5O_{15}$ ceramics were synthesized by an ordinary solid-state sintering method, and their microstructures, dielectric, piezoelectric and ferroelectric properties were studied in detail. The effects of the substitutions on the phase transition were also investigated.

## 2. Experimental

The $Sr_{2-x}Ca_xNaNb_5O_{15}$ + $y$ wt% $MnO_2$ (abbreviated as SCNNM-$x$/$y$) ceramics were prepared by the conventional ceramic fabrication technique. $SrCO_3$, $Na_2CO_3$, $CaCO_3$, $Nb_2O_5$, $MnO_2$ with the purity of over 99.9% were used as raw materials. The powders in stoichiometric ratio of $Sr_{2-x}Ca_xNaNb_5O_{15}$ were ball-milled for 24 h and calcined at 1150 °C for 12 h. After the calcination, $MnO_2$ was added. The resulting mixture was ball-milled again for 24 h and mixed thoroughly with a PVA binder solution, and then pressed into pillar with dimension 13 mm and thickness 20 mm under a uniaxial pressure of 100 Mpa. The compacted pillar samples were sintered at 1230–1300 °C for 3–7 h in air. The pillar samples were cut in the direction parallel to the pressing direction. The bulk samples were then machined, polished and coated golden paste on the large surfaces as electrodes. The ceramics were poled under a dc filed of about 3 kV/mm at 200 °C in a silicone oil bath for 30 min.

The bulk densities $\rho$ of samples were measured by the Archimedes method. The crystal structures of sintered samples were confirmed using an X-ray diffraction (XRD) meter with a nickel-filtered Cu-Kα radiation (Bruker D8 Discover). The microscopy was observed using a scanning electron microscopy (SEM,JSM 6500 F). The relative permittivity $\varepsilon_r$ and loss tangent $\tan\delta$ were measured as a function of temperature using an impedance analyzer (Agilent 4284A). A conventional Sawyer–Tower circuit was used to measure the polarization hysteresis ($P$–$E$) loop at 5 Hz. The piezoelectric coefficient $d_{33}$, the electromechanical coupling factors $k_p$ and $k_t$ were determined by the resonance and anti-resonance frequency method according to IEEE standard 176 using an impedance analyzer (Agilent 4294 A).

## 3. Results and discussions

The XRD patterns of the SCNNM-$x$/0.5 and SCNNM-0.05/$y$ ceramics in the $2\theta$ range of 20–60° are shown in Fig. 1. All the ceramics possess a pure tungsten–bronze structure, indicating that $Ca^{2+}$ and Mn ions have diffused into the $Sr_2NaNb_5O_{15}$ lattices to form a new homogeneous solid solution. As the sintering temperature is high up to 1230 °C, Mn ions may exist in the SCNNM structure in two valence states: $Mn^{3+}$ with a radius of 0.66 Å and $Mn^{2+}$ with radius of 0.80 Å. $Nb^{5+}$ has a radius of 0.69 Å which is close to 0.66 Å of $Mn^{3+}$ and 0.80 Å of $Mn^{2+}$, and smaller than $Sr^{2+}$(1.44 Å), $Ca^{2+}$(1.34 Å) and $Na^{+}$(0.97 Å). Therefore, according to the principles of crystal chemistry and radius matching ruler, $Mn^{3+}$ or $Mn^{2+}$ most likely enter into the A-sites for substituting $Na^+$ and B-sites for substituting $Nb^{5+}$, with $Ca^{2+}$ substituting $Sr^{2+}$. Fig. 1(b) shows the enlarged XRD patterns of the ceramics in the ranges of $2\theta$ from 27° to 33°. At $x \geq 0.20$, the diffraction peaks (4 1 0) and (3 1 1) both split into two peaks, suggesting that the ceramics have a tendency to transform into another phase, e.g., orthorhombic, at high $Ca^{2+}$ substitution levers [23]. It has been reported that the crystal structure of SCNN ceramics is tetragonal tungsten–bronze phase at room temperature, because it suppressed the tetragonal–orthorhombic phase transition and thus the tetragonal phase is maintained [17]. Together with these results, it suggests that the orthorhombic and tetragonal phases coexist in the SCNNM ceramics with $x \geq 0.20$ at room temperature. It can be noted that the diffraction peaks, especially, the (2 1 1) and (3 1 1) peaks shift slightly to higher $2\theta$ as $x$ increases. This may be attributed to the smaller ionic radius of $Ca^{2+}$ as compared to $Sr^{2+}$. It has been also observed that the XRD patterns of the ceramics with different $y$ are similar (Fig. 1(c)). This indicates that the $MnO_2$ addition has no significantly effect on the crystal structure. Fig. 2 shows the scanning electron microscopy (SEM) micrographs of the SCNNM-$x$/$y$ ceramics with $x$/$y$ = 0.05/0.5, 0.25/0.5, 0.35/0.5, 0.05/0, 0.05/1.0, and 0.05/1.5. All the ceramics are dense and well crystallized, except for SCNNM-0.05/0 and -0.05/1.5. For the SCNNM-$x$/0.5 samples, there is an inhomogeneous grain size distribution, such as the grains have a bimodal grain size distribution, with big grains being surrounded by small grains. For the ceramic with $x$ = 0.25 (Fig. 2(b)), as an example, the average grain sizes are 12.2 and 5.1 μm for the big and small grains, respectively. It can be also seen that with the increasing of $x$ (i.e., the concentration of $Ca^{2+}$), the grains are nonuniform and the grain size remains almost unchanged, suggesting that the $Ca^{2+}$ substitution has no significant effects on the densification of the ceramics. Unlike $Ca^{2+}$, Mn ions have much more significant effects on the sintering of the SCNNM ceramics (Fig. 2(e–f)). Although the sintering temperature is high (1300 °C), the ceramic of SCNNM-0.05/0 has a relatively loose structure and a number of pores can be found (Fig. 2(d)). However, after the addition of 0.5 wt% $MnO_2$, the ceramics can be well sintered at a low sintering temperature of 1230 °C and a dense microstructure with enlarged grains is developed (Fig. 2(a)). Furthermore, the size of the grains is generally found obviously increased with the $MnO_2$ additive. One possible reason to trigger the grain growth is that the $MnO_2$ additive acting as the liquid phase during sintering above 1200 °C. The increasing grain size with the $MnO_2$ additive also implies that Mn ions were homogeneously dissolved into SCNNM grains within the solubility limit, while, the excess Mn ions accumulated at the grain boundaries to facilitate the liquid-phase sintering. However, when the amount of $MnO_2$ addition is over 1.0 wt%, some Mn ions may accumulate in the grain boundaries, and result in a pinning effect on the domain wall, hindering the motion of the domain [24]. As shown in Fig. 2(f), cracks are found in the SCNNM-0.05/1.5 ceramic and the grain size varies considerably with anomalous grain size distribution. This may be attributed to the reduction in the mobility of the grain boundary and the weakness in the mass transportation after the further addition of $MnO_2$. It is clearly seen that with a small amount of $MnO_2$ (0.3–1.0 wt%) doping, the SCNNM ceramics can be well sintered at a relatively low temperature. However, further addition of $MnO_2$ (over 1.0 wt%) would inhibit grain growth due to the accumulation of Mn ions at the grain boundaries, resulting a poor sintering performance of the ceramics.

The bulk density $\rho$, the axial ratio $\sqrt{10}c/a$, and the lattice unit volume $V$ of sintered SCNNM ceramics are shown in Fig. 3. As shown in Fig. 3(a), the bulk density $\rho$ for the SCNNM-$x$/0.5 ceramics is generally found decreases with increasing $x$ (the concentration of $Ca^{2+}$). On the other hand, the value axial ratio $\sqrt{10}c/a$ first increases slightly and decreases and then remains almost unchanged at $x \geq 0.20$. At the same time, the lattice unit volume $V$ first increases and then decreases gradually with increasing $x$. The changes in the axial ratio $\sqrt{10}\,c/a$, and the lattice unit volume $V$ should be related to a small difference in the ionic radii between $Ca^{2+}$ (1.34 Å) and $Sr^{2+}$ (1.44 Å). Moreover, in the tungsten–bronze system, the value of the axial ratio $\sqrt{10}\,c/a$ is usually used to evaluate the distortion of the $NbO_6$ octahedron. As $Ca^{2+}$ entered $Sr^{2+}$ site, the A-site disorder degrees and local compositional fluctuation may increase, thus giving rise to a normal phase transition. As shown in Fig. 3(b), it has been observed that the SCNNM-0.05/0 (i.e., SCNN) ceramic sintered at 1300 °C for 7 h has a low bulk density of 4.65 g/cm$^3$. However, after the doping of 0.3–0.5 wt% $MnO_2$, the SCNNM ceramics give a high density over 4.86 g/cm$^3$ even though sintered at a relatively low temperature of 1230 °C for 3 h. Furthermore, the axial ratio $\sqrt{10}\,c/a$, and the lattice unit volume $V$ for SCNNM-0.05/$y$ ceramics are generally found to change slightly with the increase of $y$ (the doping lever of $MnO_2$). On the basis of these results and SEM observations, it is clearly seen that $Ca^{2+}$ has no appreciable influence on the microstructure of the ceramics, while, the addition of $MnO_2$ effectively decreases the sintering temperature, produces a large-grained microstructure, and promotes the densification of the ceramics.

Fig. 4 shows the temperature dependence of the dielectric constant $\varepsilon_r$ for the SCNNM-$x$/0.5 ceramics at 10 kHz as a function of temperature over the range of −200 to 350 °C. Similar to pure SCNN ceramic, the SCNNM-$x$/0.5 ceramics (i.e., SCNN ceramics with 0.5 wt% $MnO_2$ doping) undergo two phase transitions: one is asso-

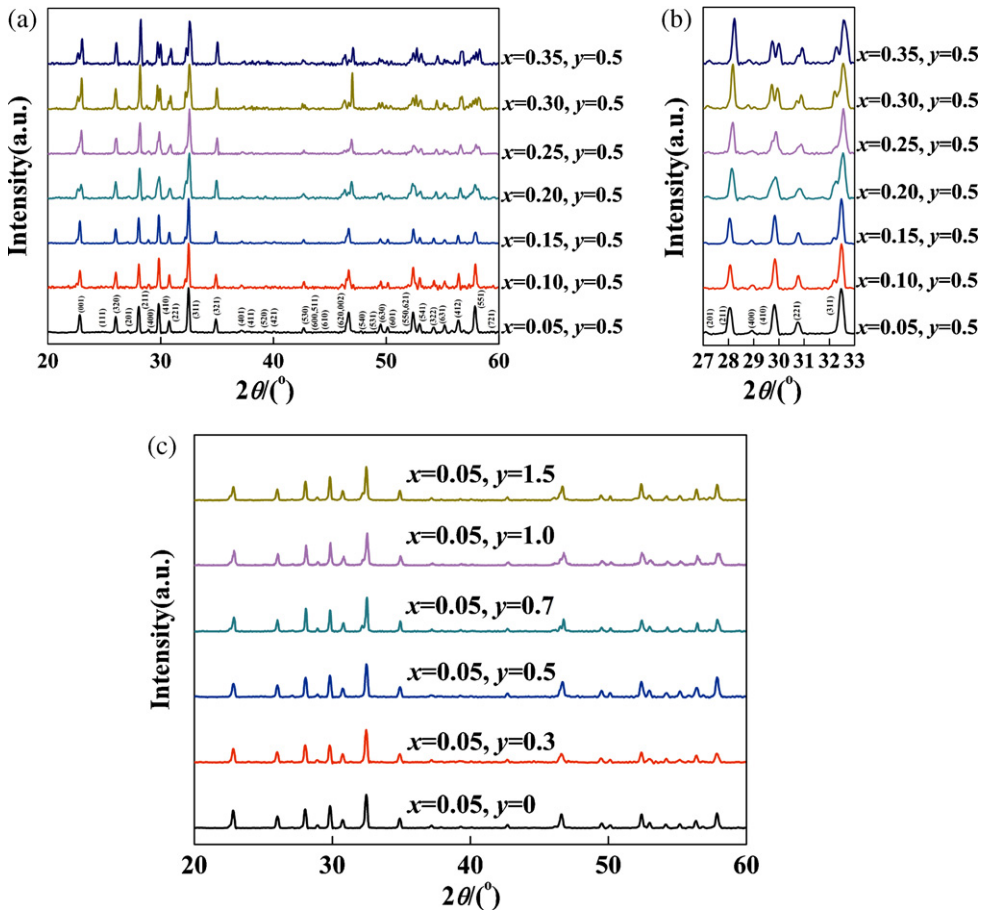


**Fig. 1.** X-ray diffraction (XRD) patterns of the SCNNM ceramics, and the enlarged XRD patterns indicating the shift of (2 1 1) and (3 1 1) peak.

ciated with the ferroelectric (4*mm*) to paraelectric (4/*mmm*) phase transition at the Curie temperature ($T_c$), and the other one is the ferroelectric (*mm*2) to ferroelectric (4*mm*) phase transition at lower temperature ($T_s$). The temperature corresponding to the maximum value of dielectric constant is named as the maximum temperature $T_m$. After the modifications with $Ca^{2+}$ and $MnO_2$, the SCNNM ceramics exhibit similar temperature dependence of $\varepsilon_r$, but with different $T_c$ and $T_s$. It can be also noted that, $T_c$ shifted to higher temperature and $T_s$ shifted to lower temperature as $x$ increasing from 0.05 to 0.35. Fig. 5(a) and (b) shows, as an example, the temperature dependence of $\varepsilon_r$ for the SCNNM-0.10/0.5, 0.35/0.5 ceramics, while, the $T_c$ and $T_s$ with concentrations of $Ca^{2+}$ ($x$) and $MnO_2$ ($y$) are summarized in Fig. 6.

As Fig. 5(a) and (b) shows, the ceramics present the main characteristic of relaxor ferroelectric, namely, strong frequency dependence of $T_m$, and different temperatures of maximum for $\varepsilon_r$ and loss tangent $\tan\delta$ at a fixed frequency [25]. Moreover, as the substitution of $Ca^{2+}$ increases, especially at $x \geq 0.20$ (as shown in Fig. 4), the ferroelectric–paraelectric phase transition became weak, and phase transition temperature $T_c$ shifted to a temperature about 300 °C, exhibiting a broaden and smooth transition peak in the plot of $\varepsilon_r$ versus temperature. These provide additional evidence for the suggestion that the orthorhombic and tetragonal phases should coexist in the ceramics with $x \geq 0.20$ near room temperature. This is consistent with the results of X-ray diffraction (Fig. 1(a) and (b)).

The variations of $T_c$ and $T_s$ with $x$ are summarized to form a phase diagram as shown in Fig. 6(a) for SCNNM-$x$/0.5 ceramics. As $x$ increases from 0.05 to 0.20, $T_c$ starts to increase from 260 to 290 °C, then has a small decrease, and then increases with the increasing of $x$, giving a maximum value of 299 °C at $x = 0.35$. Unlike $T_c$, $T_s$ first decreases, then increases and comes to a highest value of 8 °C at $x = 0.20$, and then decreases rapidly with the addition of $Ca^{2+}$. These are attributed to a partial substitution of A-site ions $Sr^{2+}$ by $Ca^{2+}$. For all the samples of SCNNM-$x$/0.5 ceramics except for $x = 0.20$, the observed $T_s$ is below 0 °C and at a range from −27 to −7 °C, suggesting that the orthorhombic and tetragonal phase coexist in the ceramics near room temperature.

Fig. 5(c) and (d) shows temperature dependence of dielectric constant $\varepsilon_r$ and the loss tangent $\tan\delta$ of SCNNM-0.05/0.3 and SCNNM-0.05/1.0 ceramics at different frequencies as a function of temperature over the range of −200 to 350 °C, respectively. It can be seen that the phase transitions for the ceramic of SCNNM-0.05/0.3 and SCNNM-0.05/1.0 are similar, and the phase transitions temperature $T_c$ and $T_s$ changed only slightly. The variations of $T_c$ and $T_s$ with $y$ for the SCNNM-0.05/$y$ ceramics are summarized to form a phase diagram as shown in Fig. 6(b). It can be seen that $T_c$ and $T_s$ both decrease rapidly as increasing $y$, and then increase, giving a minimum value of 237and −26 °C at $y = 0.10$, respectively. Compared with pure SCNN ceramic, the $T_c$ and $T_s$ of SCNNM ceramics both shift to lower temperature.

The diffuseness of a phase transition can be determined from the modified Curie–Weiss law $1/\varepsilon - 1/\varepsilon_m = C^{-1}(T - T_m)^{\gamma}$, where $\varepsilon_m$ is the maximum value of dielectric constant at the phase transition temperature $T_m$, $\gamma$ is the degree of diffuseness, and $C$ is the Curie-like constant. The $\gamma$ can have a value ranging from 1 for a normal ferroelectric to 2 for an ideal relaxor ferroelectric. Fig. 7 shows the plots of $\ln(1/\varepsilon - 1/\varepsilon_m)$ vs $\ln(T - T_m)$ for the SCNNM ceramics. As shown in Fig. 7(a), as $x$ increases from 0.05 to 0.35, $\gamma$ decreases obviously from 1.79 to 1.21 for the SCNNM-$x$/0.5 ceramics. This suggests

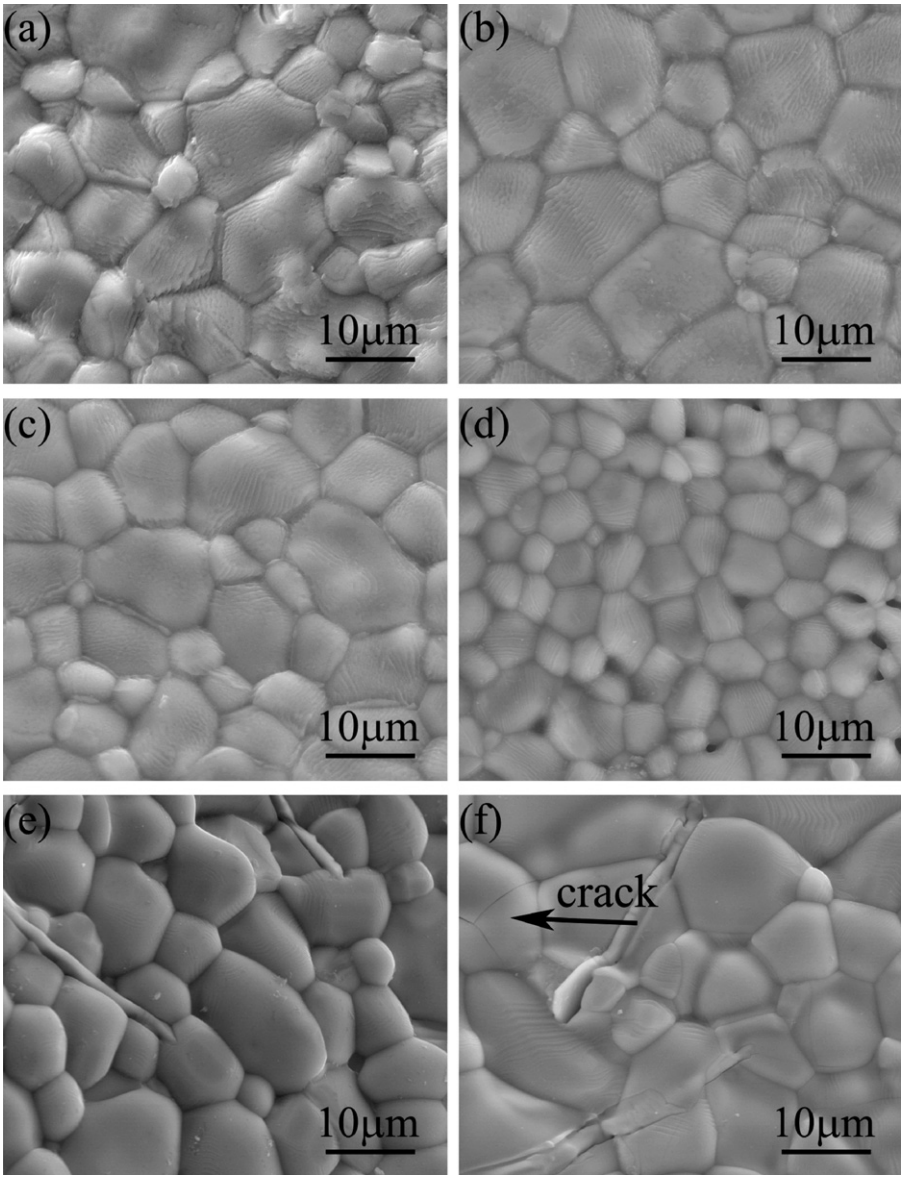


**Fig. 2.** SEM micrographs of the SCNNM-$x$/$y$ ceramics: (a) $x = 0.05$, $y = 0.5$, sintered at 1230 °C for 3 h; (b) $x = 0.25$, $y = 0.5$, sintered at 1230 °C for 3 h; (c) $x = 0.35$, $y = 0.5$, sintered at 1230 °C for 3 h; (d) $x = 0.05$, $y = 0$, sintered at 1300 °C for 7 h; (e) $x = 0.05$, $y = 0.10$, sintered at 1230 °C for 3 h; (f) $x = 0.05$, $y = 0.15$, sintered 1230 °C for 3 h.

that the substitution of $Ca^{2+}$ makes the ceramic have transformed gradually from a relaxor ferroelectric to a normal ferroelectric, thus exhibiting a weakened and broadened transition peak in the plot of $\varepsilon_r$ versus temperature, as shown in Fig. 5(a) and (b). For the SCNNM-$x$/0.5 ceramics, $Ca^{2+}$ (1.34 Å) substitute the A-site ions $Sr^{2+}$ (1.44 Å). As the radius difference between the cations increases with increasing of smaller $Ca^{2+}$ substitution for lager $Sr^{2+}$, the octahedral tilting likely becomes easier, which formed more stable polar clusters, then the coupling between polar clusters becomes stronger and makes the ceramics change from a diffused feature into a normal ferroelectric phase transition [26,27]. The values of $\gamma$ for all the SCNNM-0.05/$y$ ceramics are higher than 1.79, and changed slightly with $y$ increasing, indicating that the $MnO_2$ substitution does not induce significant changes in the phase transition, and the SCNNM-0.05/$y$ ceramics are close to ideal relaxor ferroelectric.

The variation of the piezoelectric coefficient $d_{33}$, electromechanical coupling factors $k_p$ and $k_t$, dielectric constant $\varepsilon_r$ and loss tangent $\tan\delta$ with $x$ for the SCNNM-$x$/0.5 ceramics are shown in Fig. 8. Poled specimens with $x = 0.30$ and 0.35 give no piezoelectric response. As shown in Fig. 8(a), the SCNNM-0.05/$y$ ceramic exhibits similar compositional dependences of $d_{33}$, $k_p$, $k_t$. All of them decrease gradually with the increasing of $x$. On another hand, the relative dielectric constant $\varepsilon_r$ (1 MHz) slightly increases with the increasing of $x$, and then decreases gradually at $x > 0.15$, giving a maximum value of 2226 at $x = 0.10$. While, the loss tangent $\tan\delta$ (1 MHz) increases slightly from 0.038 to 0.051, with $x$ increasing from 0.05 to 0.15, and then starts to decrease at $x = 0.20$ (Fig. 8(b)). It should be noted that the ceramics with $x = 0.05$ exhibit excellent characteristics such as $d_{33}$ (~190), $k_p$ (~13.4%), $k_t$ (~36.5%), and high $\varepsilon_r$ (~2123) and low loss tangent $\tan\delta$ (~0.038).

Fig. 9 shows the variations of $d_{33}$, $k_p$, $k_t$, $\varepsilon_r$, and the loss tangent $\tan\delta$ with $y$ for the SCNNM-0.05/$y$ ceramics. It can be noted that the observed $d_{33}$, $k_p$, $k_t$, and $\varepsilon_r$ exhibit similar dependences on $y$, i.e., first increases steeply with $y$ increasing from 0 to 0.5, and then decreases, they all reach an optimum value, being 190 pC/N, 13.4%, 36.5%, 2123 at $y = 0.5$, respectively. At the same time, the loss tangent $\tan\delta$ remains at a relatively low value ($\leq$0.055) in the range of $y$ from 0 to 1.5. However, without $MnO_2$ doping, the SCNNM-0.05/0 ceramic has a poor density and weak piezoelectricity ($\rho = 4.53$ g/cm$^3$, $d_{33} = 51$ pC/N, $k_p = 6.9\%$, $k_t = 19.2\%$). After

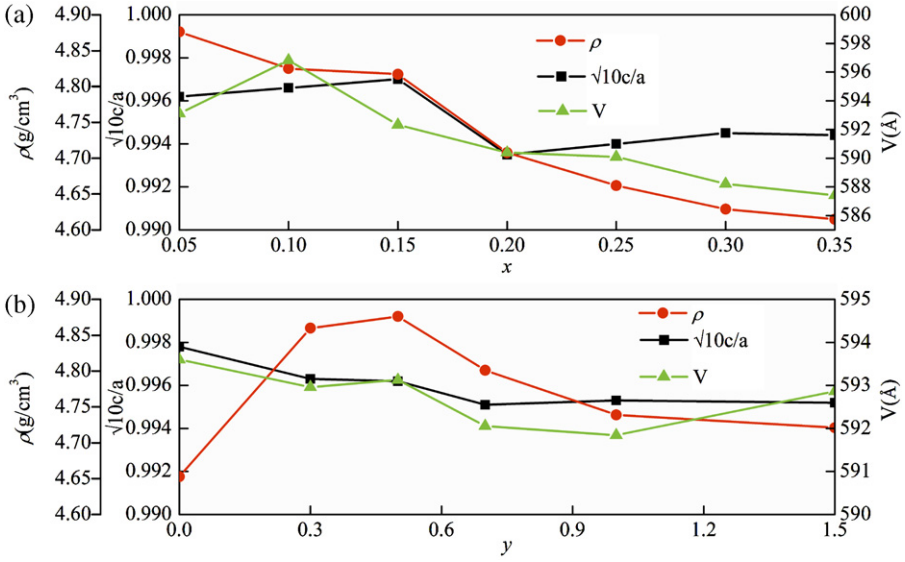


**Fig. 3.** Variations of the density $\rho$, the axial ratio $\sqrt{10}\,c/a$, and the volume for (a) SCNNM-$x$/0.5 ceramics and (b) SCNNM-0.05/$y$ ceramics.

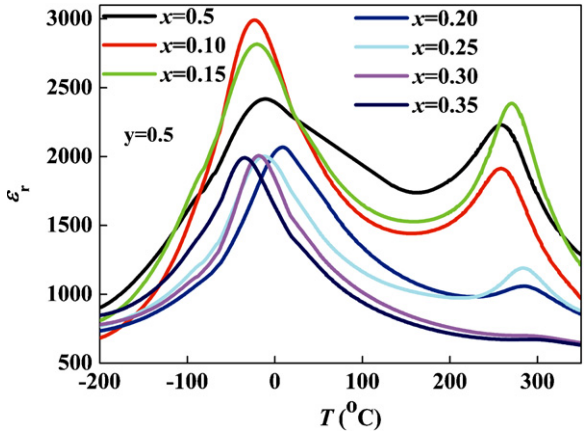


**Fig. 4.** Dielectric constant $\varepsilon_r$ of the SCNNM-$x$/0.5 ceramics as a function of temperature at 10 kHz.

the use of $MnO_2$ additive (0.3–0.5 wt%), the density, the dielectric and piezoelectric properties are considerably enhanced. These indicate that $MnO_2$ is an effective sintering aid for improving the densification (Fig. 2(b)) and plays an important role in improvement of piezoelectric and dielectric properties (Fig. 8). Moreover, the increase in $\varepsilon_r$ can be understood by the increase in the grain size with $MnO_2$ addition. The $MnO_2$ additive enhances the average grain size, making the domain wall motion easier, resulting in an increased dielectric coefficient. Meanwhile, the loss tangent $\tan\delta$ decreases from 0.055 to 0.028 with $y$ increasing from 0 to 0.10, and then increases slightly from 0.028 to 0.034 at $y \geq 0.10$. For a small amount of $MnO_2$ additive (0.3–1.0 wt%), the systems show simultaneously "softening" and "hardening", which resulting in the variations of piezoelectric properties [28]. The "soft" and "hard" dopant mechanisms of $MnO_2$ in the ceramics will be shown in the next section. Further addition of $MnO_2$ above 1.0 wt% led to the decrease of piezoelectricity because of nonuniformity of the microstructure.

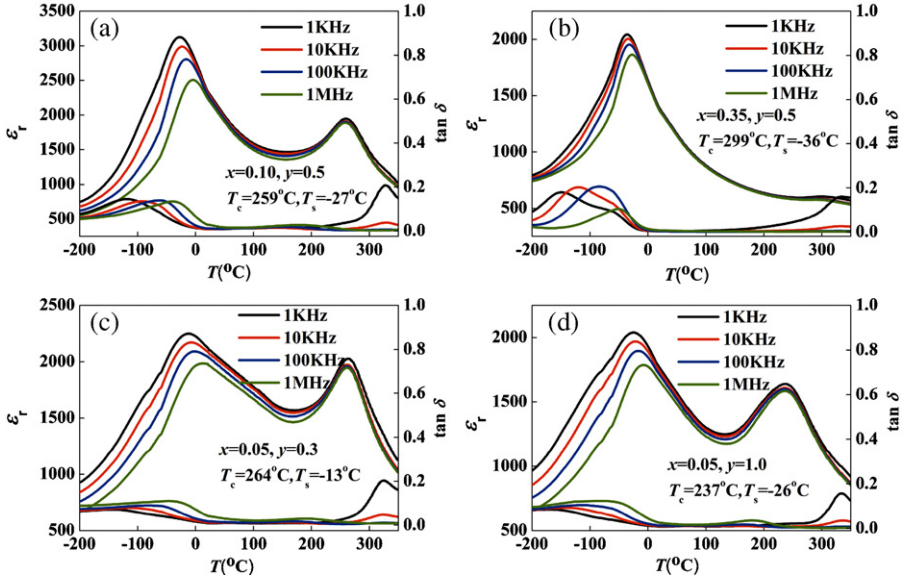


**Fig. 5.** Dielectric constant $\varepsilon_r$ and loss tangent $\tan\delta$ of SCNNM ceramics as a function of temperature: (a) $x = 0.10$, $y = 0.5$; (b) $x = 0.35$, $y = 0.5$; (c) $x = 0.05$, $y = 0.3$; (d) $x = 0.05$, $y = 0.10$.

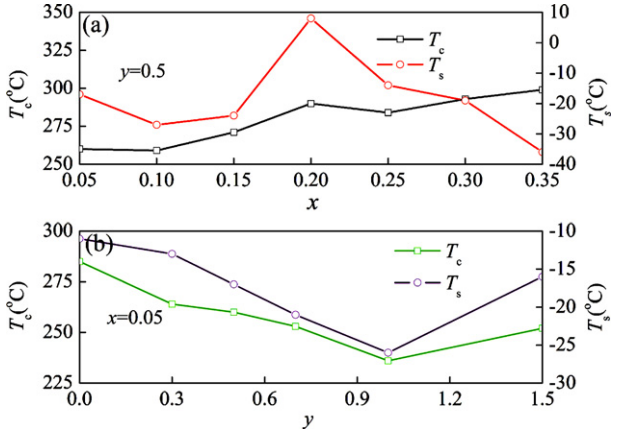


**Fig. 6.** Variations of $T_c$ and $T_s$ of (a) SCNNM-$x$/0.5 ceramics, with $x$ = 0.05–0.35, and of (b) SCNNM-0.05/$y$ ceramics, with $y$ = 0–1.5.

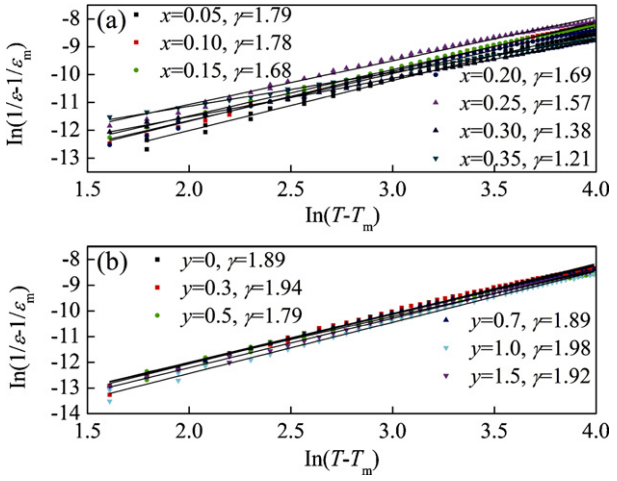


**Fig. 7.** Plot of $\ln(1/\varepsilon - 1/\varepsilon_m)$ vs $\ln(T - T_m)$ for the SCNNM-$x$/$y$ ceramics. The symbols denote experiment data, while the solid lines denote the least-squares fitting line to the modified Curie–Weiss law.

Figs. 10(a) and 11(a) show the typical $P$–$E$ hysteresis loops of SCNNM-$x$/0.5and SCNNM-0.05/$y$ ceramics, measured under an electric field of about 3 kV/mm at room temperature. The variations of the remanent polarization $P_r$ and coercive filed $E_c$ with $x$ and $y$ are shown in Figs. 10(b) and 11(b), respectively. It is clearly

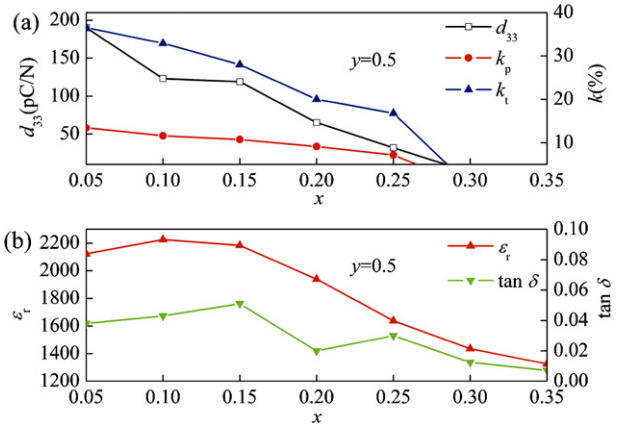


**Fig. 8.** (a) Variations of piezoelectric coefficient $d_{33}$ and electromechanical coupling factors $k_p$ and $k_t$ with $x$ for the SCNNM-$x$/0.5 ceramics; (b) variations of the dielectric constant $\varepsilon_r$ and loss tangent tan $\delta$ with $x$ for the SCNNM-$x$/0.5 ceramics.

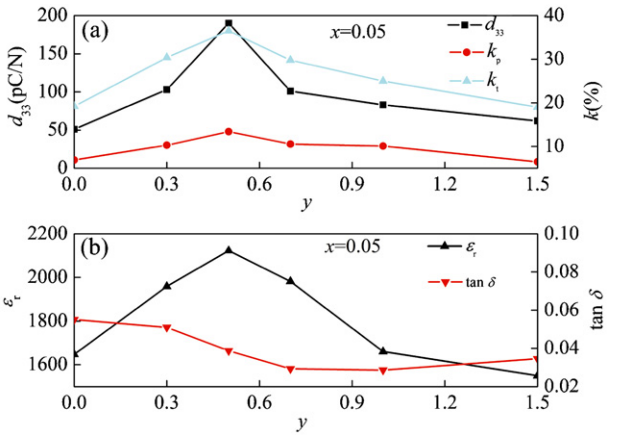


**Fig. 9.** (a) Variations of piezoelectric coefficient $d_{33}$ and electromechanical coupling factors $k_p$ and $k_t$ with $y$ for the CNNM-0.05/$y$ ceramics; (b) variations of the dielectric constant $\varepsilon_r$ and the loss tangent tan $\delta$ with $y$ for the SCNNM-0.05/$y$ ceramics.

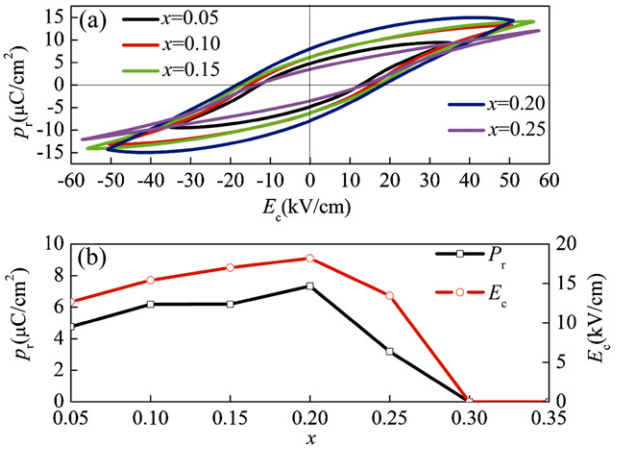


**Fig. 10.** (a) $P$–$E$ hysteresis loops of the SCNNM-$x$/0.5 ceramics with different $x$; (b) variations of the remanent polarization $P_r$ and coercive field $E_c$ with $x$ for the SCNNM-$x$/0.5 ceramics.

to see that for the SCNNM-$x$/0.5 ceramics at $x$ = 0.05–0.25, the $P$–$E$ loops are slim, slanted, and well saturated. Similar to the piezoelectric properties, specimens with composition of $x$ = 0.30 and 0.35 give no ferroelectric properties. For the SCNNM-$x$/0.5 ceramics, the

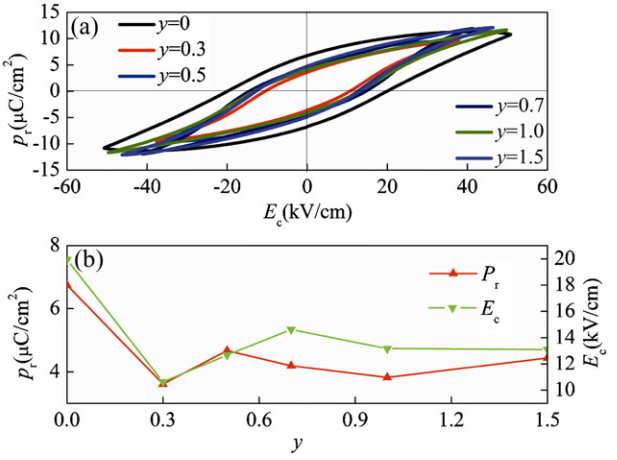


**Fig. 11.** (a) $P$–$E$ hysteresis loops of the SCNNM-0.05/$y$ ceramics with different $y$; (b) variations of the remanent polarization $P_r$ and coercive field $E_c$ with $y$ for the SCNNM-0.05/$y$ ceramics.

observed $E_c$ increases gradually with $x$ increasing from 0.05 to 0.20, and then starts to decrease rapidly, giving a maximum value of 18.22 kV/cm at $x = 0.20$. The remanent polarization $P_r$ shows similar dependence on $x$, i.e., first increases from 4.76 to 7.34 μC/cm$^2$ as $x$ increases from 0.05 to 0.20, and then decreases linearly at $x \geq 0.20$. These clearly show that the substitution of $Ca^{2+}$ has enhanced the ferroelectric properties first, and then weakened the ferroelectric properties of the SCNNM ceramics. The enhancement of remnant polarization $P_r$ with $Ca^{2+}$ additive may be related to the enhanced domain wall mobility, which allows for more complete domain switching of the ceramics. Similarly, all the SCNNM-0.05/$y$ ceramics exhibit well-saturated $P$–$E$ loops under an electric field of about 3 kV/mm. Fig. 11(b) shows the remnant polarization $P_r$ and coercive filed $E_c$ of the SCNNM-0.05/$y$ ceramics as a function of $y$. It can be seen that $P_r$ decreases from 6.75 to 3.14 μC/cm$^2$, as $y$ increases from 0 to 0.3, and then increases slightly and becomes saturated at about 3.80 μC/cm$^2$. $E_c$ is lowered greatly from 19.94 to10.63 kV/cm, as $y$ increases from 0 to 0.3, and then increases and decreases slightly. Compared with the pure SCNN ceramics, the SCNNM ceramics have lower coercive filed $E_c$ and relatively good ferroelectric properties. The observed dielectric, piezoelectric and ferroelectric properties show that Mn ions can cause both "soft" and "hard" doping effects simultaneously in SCNNM-0.05/$y$ ceramics. In a sense, at low $MnO_2$ additive ration (≤0.5 wt%), Mn ions go to $Na^+$ sites in SCNNM. It is well known that $Na_2O$ is volatile at high temperature. $Na^+$ in SCNNM may leave the ceramic and form some vacancies in the lattice during the sintering process. The substitution of $Na^+$(0.97 Å) by higher valence of $Mn^{3+}$ (0.66 Å) and $Mn^{2+}$ (0.80 Å), creates cation vacancies, thus, Mn ions act as "donors". Ions in the lattice are transferred easier due to the presence of vacancies, which results in the easy movement of domain walls, which makes the ferroelectric ceramic to become "softer". When the $MnO_2$ additive ratio between 0.5 and 1.0 wt%, B-site ions $Nb^{5+}$ (0.69 Å) may be substituted by $Mn^{3+}$ (0.66 Å), thus causes a fast drop in $d_{33}$, $k_t$, $\varepsilon_r$ and a slight decrease in $P_r$, indicating that $MnO_2$ additives have played as a hard agent in the SCNNM ceramics. In conclusion, Mn doping in SCNNM ceramics produced both soft and hard effects, caused by the multivalence nature of Mn ions, which get into different sites in the tungsten–bronze structure.

## 4. Conclusions

Lead-free SCNNM-$x$/$y$ piezoelectric ceramics have been prepared by an ordinary sintering technique, and their microstructures, phase transitions, and electrical properties have been investigated in detail. Our results reveal that $Ca^{2+}$and Mn ions have diffused into $Sr_2NaNb_5O_{15}$ lattices to form a solid solution with tungsten–bronze structure. The substitution of $Ca^{2+}$decreases $d_{33}$, $k_p$ and $k_t$, and makes the ceramics become less relaxor. A small amount of $MnO_2$ (0.3–1.0 wt%) effectively promotes the densification and decreases the sintering temperature of the ceramics. The densification, "hard" and "soft" effects of $MnO_2$ doping should be attributed to the strong dielectricity and high piezoelectricity of the ceramics. For the ceramics with $x = 0.05$, $y = 0.5$, the piezoelectric and dielectric properties become optimum, giving $d_{33} = 190$ pC/N, $k_p = 13.4\%$, $k_t = 36.5\%$, $\varepsilon_r = 2123$, loss tangent $\tan\delta = 0.038$ and the Curie temperature $T_c = 260\,^\circ$C. Results show that $MnO_2$ doped $Sr_{2-x}Ca_xNaNb_5O_{15}$ ($x = 0.05$–$0.35$) ceramics are one of the good candidates for lead-free piezoelectric material.

## Acknowledgments

This work was supported by the Beijing Municipal Commission of Education Foundation of China (no. JC00615200901). The authors would like to thank Dr. X. Du and Prof. Y. Zhang for their help in experiment.

## References

[1] D. Zhou, M. Kamlah, J. Eur. Ceram. Soc. 25 (2005) 2415.
[2] T.R. Shrout, S.J. Zhang, J. Electroceram. 19 (2007) 113.
[3] B.-J. Chu, D.-R. Chen, G.-R. Li, Q.-R. Yin, J. Eur. Ceram. Soc. 22 (2002) 2115.
[4] Y. Hou, M. Zhu, L. Hou, J. Liu, J. Tang, H. Wang, H. Yan, J. Cryst. Growth 273 (2005) 500.
[5] D. Lin, K.W. Kwok, H.L.W. Chan, J. Alloys Compd. 481 (2009) 310.
[6] S. Ke, H. Fan, H. Huang, H.L.W. Chan, S. Yu, J. Appl. Phys. 104 (2008) 024101.
[7] Y. Yang, Y. Liu, J. Meng, Y. Huan, Y. Wu, J. Alloys Compd. 453 (2008) 401.
[8] T. Maiti, R. Guo, A.S. Bhalla, Appl. Phys. Lett. 90 (2007) 182901.
[9] Q. Yin, S. Yuan, Q. Dong, C. Tian, J. Alloys Compd. 491 (2010) 340.
[10] Y. Guo, K. Kakimoto, H. Ohsato, Mater. Lett. 59 (2005) 241.
[11] R.R. Neurgaonkar, J.R. Oliver, W.K. Cory, L.E. Cross, D. Viehland, Ferroelectrics 160 (1994) 265.
[12] X.L. Zhu, X.M. Chen, X.Q. Liu, X.G. Li, J. Appl. Phys. 105 (2009) 124110.
[13] R.R. Neurgaonkar, W.K. Cory, J.R. Oliver, E.J. Sharp, G.L. Wood, M.M. Miller, W.W. Clark, G.J. Salamo, Mater. Res. Bull. 23 (1988) 1459.
[14] P.B. Jamieson, S.C. Abrahams, J.L. Bernstein, J. Chem. Phys. 50 (1969) 4352.
[15] T. Kimura, S. Miyamoto, T. Yamaguchi, J. Am. Ceram. Soc. 73 (1990) 127.
[16] M.H. Francombe, Acta Cryst. 13 (1960) 131–140.
[17] R.-J. Xie, Y. Akimune, J. Mater. Chem. 12 (2002) 3156.
[18] R.-J. Xie, Y. Akimune, K. Matsuo, T. Sugiyama, N. Hirosaki, T. Sekiya, Appl. Phys. Lett. 80 (2002) 835.
[19] R. Tipakontitikul, Y. Suwan, A. Niyompan, Ferroelectrics 381 (2009) 144.
[20] Y. Hou, M. Zhu, F. Gao, H. Wang, B. Wang, H. Yan, C. Tian, J. Am. Ceram. Soc. 87 (2004) 847.
[21] D. Lin, K.W. Kwok, H.L.W. Chan, Mater. Chem. Phys. 109 (2008) 455.
[22] L.X. He, C.E. Li, J. Mater. Sci. 35 (2000) 2477.
[23] C. Zhou, X. Liu, W. Li, C. Yuan, J. Alloys Compd. 478 (2009) 381.
[24] H.E. Mgbemere, R.-P. Herber, G.A. Schneider, J. Eur. Ceram. Soc. 29 (2009) 1729.
[25] J. Shi, W. Yang, J. Alloys Compd. 472 (2009) 267.
[26] I.A. Santos, D.U. Spinola, D. Garcia, J.A. Eiras, J. Appl. Phys. 92 (2002) 3251.
[27] X.L. Zhu, S.Y. Wu, X.M. Chen, Appl. Phys. Lett. 91 (2007) 162906.
[28] G. Li, L. Zheng, Q. Yin, B. Jiang, W. Cao, J. Appl. Phys. 98 (2005) 064108.